Energy Conversion and Management 270 (2022) 116268

Contents lists available at ScienceDirect

Energy Conversion and Management

journal homepage: www.elsevier.com/locate/enconman

Thermodynamic analysis of a novel adsorption-type trans-critical compressed carbon dioxide energy storage system

Tianhang Zhang [a], Jianmin Gao [a,*], Yu Zhang [a,*], Jin Zhang [a], Qiaoqun Sun [b], Qian Du [a], Zhipei Tang [a], Yirui Peng [a]

[a] School of Energy Science and Engineering, Harbin Institute of Technology, No. 92, West Dazhi Street, Harbin 150001, China
[b] School of Aerospace and Construction Engineering, Harbin Engineering University, No. 145, Nan Tong Street, Harbin 150001, China

ARTICLE INFO

Keywords:
Compressed carbon dioxide energy storage
Thermodynamic simulation
Sensitivity analysis
Carbon dioxide adsorption

ABSTRACT

Compressed CO_2 energy storage technology is a feasible resolution to stabilize the fluctuation of renewable energy output and has significant development prospects. The main challenge currently facing is how to achieve high-density storage of low-pressure CO_2. To get rid of the engineering application limitations caused by low-pressure CO_2 liquefaction storage and large-scale cave storage, a new type of adsorption trans-critical compressed CO_2 energy storage system is proposed in this paper. Using Fe-MOR(0.25) as an adsorbent, the storage density of CO_2 can reach 390.94 kg/m^3 at 298 K and 0.1 MPa. The thermodynamic simulation is carried out based on the first and second laws of thermodynamics. The results demonstrate that the system round trip efficiency, exergy efficiency, and energy storage density under the design conditions are 66.68 %, 67.79 %, and 12.11 kWh/m^3, respectively. The results of sensitivity analysis indicate that the storage pressure and storage temperature of the high-pressure tank have compound effects on the system, and they are the key parameters affecting the performance of the system. Releasing pressure at critical points can cause abrupt changes in system performance. Heat exchanger effectiveness, compressor, and turbine isentropic efficiency improvements positively affect the system performance.

1. Introduction

With the increasing environmental pollution and greenhouse effect caused by fossil fuels, speeding up the establishment of a new energy system with renewable energy as the main source has become the theme of the times [1,2]. However, the new energy sources represented by wind power and photovoltaic have inherent properties such as volatility and intermittency, and cannot provide a continuous and steady power supply [3]. The solution to the issue lies in developing an energy network with the deep coupling of source-grid-load-storage [4]. Energy storage technology applies to multiple scenarios such as power supply side, grid side, and load side, with functions such as “peak shaving and valley filling” and “fluctuations smoothing” and has been developing rapidly in recent years [5,6].

Due to the restrictions of technical characteristics, only pumped hydro storage and compressed gas energy storage can be installed on a large scale [7]. Pumped hydro storage requires strict geographic conditions, making site selection hard, and development has tapered off in recent years [8]. Compressed gas energy storage(CGES) has the advantages of a short construction period, a long lifespan, and stable performance, making it one of the most promising technologies [9].

Most conventional CGES use air as the working medium, namely compressed air energy storage (CAES) [10]. According to the working principle, the CAES operation process can divide into two stages: energy storage and energy release. During the low load period of the grid, the compressor unit compresses the air to a high temperature and high-pressure state and stores it in the storage chamber after cooling. In the peak load period of the grid, the high-pressure air released from the storage chamber enters the turbine after reheating to do work.

To improve the power production capacity of the turbine, the conventional CAES needs to use supplemental combustion in the energy release stage. The commercially operating Huntorf (Germany) and Mclntosh (USA) power plants use natural gas for combustion, resulting in cycle efficiencies of 42 % and 49 %, respectively, and still produce large amounts of CO_2 emissions [11,12]. To overcome the above dilemma, scholars have proposed the advanced adiabatic compressed air energy storage (AA-CAES) technology [13]. The principle of AA-CAES is

* Corresponding authors.
E-mail addresses: yagjm@hit.edu.cn, zhang.y@hit.edu.cn (Y. Zhang).

https://doi.org/10.1016/j.enconman.2022.116268
Received 24 June 2022; Received in revised form 9 September 2022; Accepted 20 September 2022
Available online 29 September 2022

Nomenclature

Symbols

$\dot{m}$	mass flow rate (kgs)
p	pressure (MPa)
S	specific entropy (kJ/kg K)
T	temperature (K)
t	time (s)
V	volume (m^3)
M	mass (kg)
EVR	energy storage density (kWh/m^3)
RTE	round trip efficiency (%)
u	thermodynamic energy (kJ/kg)
h	enthalpy (kJ/kg)
$\dot{Q}$	thermal power (kW)
$\dot{E}$	exergy flow rate (kW)
$\dot{W}$	electrical power (kW)

Abbreviations

CO_2	carbon dioxide
CGES	compressed gas energy storage
CAES	compressed air energy storage
AA-CAES	advanced adiabatic compressed air energy storage
CCES	compressed CO_2 energy storage
TC-CCES	trans-critical compressed CO_2 energy storage
A-TC-CCES	adsorption-type trans-critical compressed CO_2 energy storage
A-LPT	adsorption-type low pressure tank
C	compressor
IC	intercooler
HPT	high pressure tank
TV	throttle valve
RH	reheater
T	turbine
P	pump
HT	hot tank
CT	cold tank
Fe	iron
MOR	mordenite

Greeks

η	efficiency (%)
ρ	density (kg/m^3)
ε	heat exchanger effectiveness (/)
β	adsorption performance of adsorbent (m^3/m^3)

Subscripts and Superscripts

es	energy storage stage
er	energy release stage
is	isentropic
in	inlet
out	outlet
i	stage number
D	destruction
EX	exergy
HE	heat exchanger
hot	hot fluid
cold	cold fluid
ideal	ideal state
k	stream number
j	component number
net	net power
0	ambient state

to store the compression heat generated in the energy storage stage in the thermal storage medium, and the air is reheated and then enters the turbine to produce work during the energy release stage [14]. AA-CAES can get rid of fossil fuels and operates more efficiently. Nevertheless, due to the low air density, AA-CAES usually requires large-capacity underground caverns as high-pressure storage chambers, which is too demanding for geographical conditions and has limited applications [15].

Carbon dioxide(CO_2) has non-flammable, high density, low viscosity, excellent heat transfer performance, a mild critical point (304.25 K, 7.38 MPa), and other properties. Thus CO_2 can be used as a substitute for air [16]. The principle of compressed CO_2 energy storage(CCES) is the same as CAES, but the exception is that CO_2 belongs to greenhouse gas and needs to be in a closed-loop, so there is a low-pressure CO_2 storage issue. Liu et al. [17] proposed a CCES with subsurface saline aquifers as gas storage chambers. The system uses different depth aquifers as high and low-pressure storage chambers. The results showed that the supercritical system has higher energy storage density, while the cross-critical system has higher cycle efficiency. Chaychizadeh et al. [18] presented a CCES based on a double underground storage chamber to improve the wind power dispatch, which improved the turbine work capacity by mixing compression heat with electrical heat storage. The cycle efficiency ranges from 55.72 to 58.16 %, and the energy storage density is 83.7–86.5 kWh/m^3 considering the wind power volatility conditions. Cao et al. [19] suggested a CCES with an abandoned mine as the high-pressure storage chamber and an underground cavern as the low-pressure storage chamber. The thermodynamic analysis suggested that the cycle efficiency of the system was up to 53.75 %. Similarly, Hao et al. [20] introduced a TC-CCES system with an integrated heat pump. By applying a heat pump to enhance the waste heat energy grade, the system cycle efficiency, energy storage efficiency, and heat storage efficiency were 66 %, 54.81 %, and 46 %, respectively. Based on the system structure of the literature [21], Fu et al. [22] used trough solar collectors instead of a combustion chamber. The cycle efficiencies of supercritical and trans-critical systems reached 77.75 % and 67.72 %, respectively. Xu et al. [23] applied submerged flexible airbags to store low-pressure CO_2. The utilization of heat return and diversion measures improved the system circulation efficiency and exergy efficiency by 13.42 % and 12.46 %, respectively, compared to the base configuration.

Nevertheless, all the studies mentioned above employed large underground caves as low-pressure gas storage chambers, which dramatically restricted the geographical application of the system. The liquefaction approach can improve the storage density of low-pressure CO_2, making it a viable solution to the issue. Wang et al. [24,25] compared three system configuration options for low-pressure CO_2 liquefaction by employing cold storage units. The results suggested that the improved system with coupled ORC has the optimal performance with cycle efficiency and energy storage density of 56.7 % and 36.06 kWh/m^3, respectively. Zhang et al. [26] investigated a system with low-pressure CO_2 condensation and evaporation through a cold storage unit. In comparison, the energy storage density of this system is 2.8 times higher than that of AA-CAES under the same conditions. Wang et al. [27] explored a TC-CCES with low-pressure CO_2 liquefaction storage. Simulation results revealed that the system cycle efficiency and energy storage density were 59.98 % and 2.6 kWh/m^3, respectively. The exergy analysis showed that the condenser exergy destruction was the greatest, accounting for 16.88 %.

Liu et al. [28] examined a system in which high and low-pressure CO_2 was stored in the liquid phase, and performed thermal and economic analyses. The multi-objective optimization results indicated that

the investment cost is 0.25$/kWh when reaching the optimal exergy efficiency of 61.39 %. Liu et al. [29] researched a system of condensing CO_2 via an injected refrigeration cycle. In addition, the turbine inlet CO_2 is heated with fluctuating electrical power. Economic analysis results suggested that the system cost per unit capacity is lower than CAES. Zhang et al. [30] introduced a CCES employing low-pressure CO_2 liquid storage. Low-pressure CO_2 phase changes were conducted using ice slurry as the heat storage medium. The kinetic energy of liquid CO_2 was recovered using a cryo-turbine with a cycle efficiency of 55.7 % at the design operating conditions. Likewise, Zhang et al. [31] suggested a CCES with the same heat storage heat exchanger to make the CO_2 phase change. The optimization results revealed that the maximum cycle efficiency and the corresponding energy storage density were 43.96 % and 17.77 kWh/m^3, respectively. Bao et al. [32] introduced a novel liquefied CCES, which achieves CO_2 condensation by liquefied natural gas and a two-stage ORC cycle. The optimal cycle efficiency and the lowest economic cost of this system are 375.49 % and 0.08 USD/kWh, respectively. Huang et al. [33] proposed a novel thermal storage configuration scheme for the low heat transfer efficiency of liquid compressed CO_2 energy storage system. By dividing and matching the heat transfer temperature gradient, the system circulation efficiency reached 57.85 %. To solve the problem of subcritical CO_2 condensation within a liquefied compressed CO_2 energy storage system, Liu et al. [34] considered the utilization of CO_2 mixed with organic fluid. The results show that the pure CO_2 system has higher circulation efficiency, while the mixing fluid system has a higher energy density. Sun et al. [35] proposed two liquefied CCES with refrigeration functions. Compared with the basic structure, the system with added recuperative cycle had better performance, and the cycle efficiency and energy storage density reached 78.66 % and 12.69 kWh/m3, respectively. Xu et al. [36] suggested a CCES-based combined heat and power system with CO_2 condensation and evaporation via methanol and water. The thermodynamic analysis results show that the improved system efficiency and capacity are 63.44 % and 16.23 MW, respectively, and the thermoelectric ratio is flexible and adjustable. To improve the operational flexibility of thermal power plants, Chae et al. [37] proposed three types of liquefied compressed CO_2 energy storage systems using steam as the heat source. The simulation results show that the maximum cycle efficiency and energy storage density are 46 % and 36 kWh/m3, respectively. Compared with the conventional CCES, the liquefied CCES has significantly improved energy storage density, but at the same time, the cycle efficiency decreased seriously.

From the literature research mentioned above, it is evident that most of the current studies usually adopt liquefaction to enhance the storage density of low-pressure CO_2. However, this would cause many challenges: (1) high storage pressure leads to a small range of pressure variation of the working mass, which reduces the work capacity; (2) a heat storage heat exchanger is usually required to condense and evaporate CO_2, resulting in an enormous heat storage heat exchanger and high investment and maintenance costs; (3) the heat storage heat exchanger has a gigantic exergy loss, which reduces system performance, etc.

CO_2 adsorption enables high-density storage of low-pressure CO_2 and has become a viable alternative to CO_2 liquefaction. Compared with chemical adsorbents, solid physical adsorbents possess the advantages of high efficiency, easy regeneration, and suitability for industrial applications [38,39]. Furthermore, the adsorbent applied in the energy storage system should have the features of low cost, high efficiency, fast adsorption and desorption rate, high stability, and excellent moisture-proof performance [40]. Zhou et al. [41] developed a self-formable CO_2 adsorbent, Fe-MOR(0.25) (where 0.25 is the molar ratio of Fe to Si in zeolite), by adding Fe ions to mordenite. The performance of adsorption of Fe-MOR(0.25) can reach 219 cm^3/cm^3 at 298 K and 0.1 MPa, which is better than previous typical adsorbents [42,43]. In addition, experimental data showed that Fe-MOR(0.25) could achieve 90 % of saturated CO_2 adsorption in 2.5 min when the adsorbent was a mixture of 15 % N2 and 85 % CO_2, so Fe-MOR(0.25) could achieve CO_2 adsorption and desorption process under dynamic conditions. In terms of engineering applications, Fe-MOR(0.25) also has the advantages of good moisture resistance, fast self-forming, and high compression resistance [41]. In summary, Fe-MOR(0.25) has excellent performance and is suitable for internal application in energy storage systems.

Based on the logical analysis mentioned above, this paper proposes a novel adsorption-type trans-critical compressed CO_2 energy storage system (A-TC-CCES) using Fe-MOR(0.25) as the base adsorbent. The main innovation of this system is that CO_2 is stored at a high density by physical adsorption at 0.1 MPa. As a result, the system does not need to rely on large underground caves and has a broader range of applications. Furthermore, the CO_2 in the system does not need to liquefy, and no heat storage heat exchanger is used, which makes the engineering application much more practical. In addition, the pressure range of CO_2 in the system is 0.1 ~ 10 MPa, which is larger than the current study, and the single-cycle storage and power supply capacity is more robust.

2. System description

The schematic diagram of the novel A-TC-CCES is exhibited in Fig. 1. The main innovation is that the low-pressure storage tank is filled with high-performance adsorbents (Fe-MOR(0.25)) to achieve high-density low-pressure CO_2 storage. Both high and low-pressure storage tanks are artificial containers, which makes the system more suitable for large-scale engineering applications.

During low load periods on the grid, the system begins to store energy. The CO_2 released from the A-LPT (state 1) is compressed in three stages (1–2, 3–4, 5–7) and cooled between stages (2–3, 4–5, 6–7) to complete the energy storage process. Supercritical CO_2 is injected into the HPT for storage. Meanwhile, cold water from the CT is pumped into the interstage coolers (IC1, IC2, IC3) to absorb the heat of compression, and hot water enters the HT for storage. In this stage, the pressure inside the HPT continues to rise as CO_2 is continuously filled, and the energy storage stage ends when the pressure reaches the upper limit.

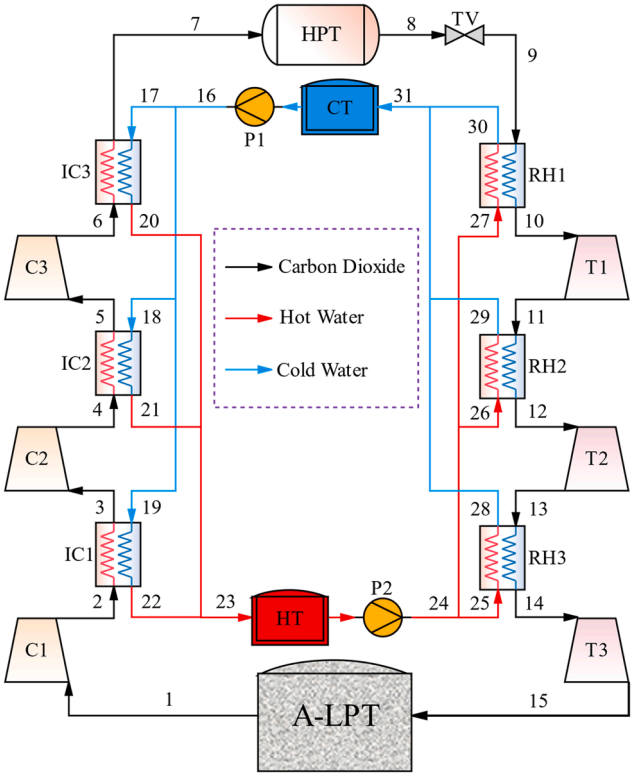

Fig. 1. Schematic diagram of A-TC-CCES.

The energy release stage starts during peak load periods of the grid. The CO_2 released from the HPT (state 8) stabilized by the TV (state 9), and then the energy release is completed by pre-stage reheating (9–10, 11–12, 13–14) and three-stage expansion (10–11, 12–13, 14–15). CO_2 exhaust gas (15) enters the A-LPT for adsorption and storage. Due to the strong electrostatic interaction between Fe-MOR (0.25) pore size and CO_2 molecules and the low temperature of CO_2 exhaust gas, the adsorption process can proceed spontaneously, so the adsorption process does not require additional special conditions [41]. The temperature of the CO_2 exhaust gas from the third stage turbine is relatively low, so the adsorption process only needs to ensure the circulating flow of CO_2 and the power consumption is negligible. During this stage, the hot water from the HT is pumped into the 3-stage reheater (RH1, RH2, RH3), and the cold water is returned to CT for storage after exotherm. In the energy release stage, the pressure inside the HPT continuously reduces due to the continuous release of CO_2, and when the pressure reaches the lower limit, the energy release stage ends. The system completes a single cycle through the above steps. Under the action of the throttle valve, the compressor and turbine operate at the design condition, i.e., the pressure ratio and expansion ratio are constant. The proposed A-TC-CCES system state point *T*-s diagram is given as Fig. 2.

3. Thermodynamic model

This section performs A-TC-CCES modeling and analysis based on the laws of thermodynamics. The device models are established in the PYTHON environment, and the thermal property parameters of the work mediums are obtained by means of COOLPROP database. To facilitate the modeling process, the following assumptions are made [20,30,44,45]:

(1) Ignore the pressure loss in pipes, heat exchangers and storage tanks.
(2) Except for the HPT, the system is in steady-state operation under design conditions.
(3) Equipment such as compressors, turbines and heat exchangers are adiabatic from the outside world, while the tanks operate as an isothermal process.
(4) The power consumption of the pump is negligible.
(5) Motor and generator efficiency is considered as 100 %.
(6) The storage temperature of A-LPT is same as the ambient temperature.

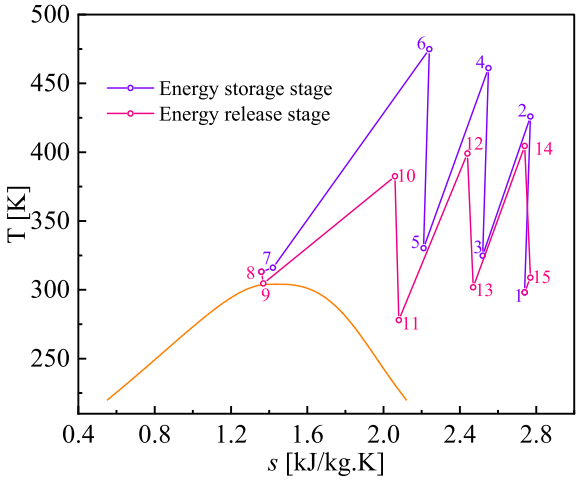

Fig. 2. *T-s* description diagram of the novel A-TC-CCES system.

3.1. Energy analysis

Based on the above assumptions, the first law of thermodynamics and the laws of conservation of mass are applied to model the devices. Each component is considered a control volume process. The detailed models are as follows.

3.1.1. Compressor model

To calculate the compressor outlet enthalpy, it is essential to establish its isentropic efficiency formula [46]:

$$\eta_C = \frac{h_{out,is} - h_{in}}{h_{out} - h_{in}} \tag{1}$$

where η represents the isentropic efficiency and the subscript *is* illustrates the isentropic process. The subscripts *in* and *out* indicate the inlet and outlet, respectively.

The system proposed in this paper has 3 stages of compressors, driven by surplus power from the grid. The power required for each compressor stage is:

$$\dot{W}_{C,i} = \dot{m}_{co_2,es}(h_{out,i} - h_{in,i}) \tag{2}$$

in which $\dot{W}_{C,i}$ represents the compressor input power of the stage i,$\dot{m}_{co_2,es}$ is the CO_2 mass flow rate in the energy storage stage, h denotes specific enthalpy.

3.1.2. Heat exchanger model

The proposed system includes 6 heat exchangers, including 3 intercoolers and 3 reheaters. The heat exchanger general energy balance model is:

$$\dot{Q}_{HE} = \dot{m}_{hot}(h_{hot,in} - h_{hot,out}) = \dot{m}_{cold}(h_{cold,out} - h_{cold,in}) \tag{3}$$

where the subscript *HE* denotes the heat exchanger abbreviation, the subscript *hot* denotes the hot fluid, the subscript *cold* denotes the cold fluid.

In this paper, the heat exchanger effectiveness model is used to calculate the fluid outlet thermodynamic parameters [47]:

$$\dot{Q}_{max} = min(\dot{m}_{hot}(h_{hot,in} - h^{ideal}_{hot,out}), \dot{m}_{cold}(h^{ideal}_{cold,out} - h_{cold,in})) \tag{4}$$

in which $\dot{Q}_{max}$ indicates the theoretical maximum heat load. $h^{ideal}_{hot,out}$ denotes the specific enthalpy that the hot fluid outlet has at the same temperature as the cold fluid inlet. Analogously, $h^{ideal}_{cold,out}$ indicates the specific enthalpy of the cold fluid when the cold fluid outlet temperature is the same as the hot fluid inlet temperature.

$$\varepsilon_{HE} = \frac{\dot{Q}_{HE}}{\dot{Q}_{max}} \tag{5}$$

where ε_{HE} denotes the heat exchanger effectiveness.

3.1.3. Throttle valve model

According to the actual working process, the throttle is an isoenthalpic process [48]:

$$h_{out} = h_{in} \tag{6}$$

3.1.4. HPT model

During the operation of HPT, the internal pressure changes continuously with the inflow or outflow of the working medium. In this paper, a constant temperature model is applied, i.e., the internal temperature of HPT is constant during the charging and discharging process. The required HPT volume is considered as the performance parameter, and the dynamic change characteristics of the internal thermodynamic parameters of the HPT are examined [49]:

$$V_{HPT} = \frac{M_{co_2}}{(\rho_{co_2,start} - \rho_{co_2,end})} \tag{7}$$

in which V means volume, M_{co_2} denotes the total mass of CO_2 charge and discharge,ρ indicates the CO_2 density. The relationship between the dynamic parameters can be obtained:

$$p(t) = f[\rho(t), T_{HPT}] \tag{8}$$

where, $p(t)$ denotes the internal pressure of HPT at time t, $\rho(t)$ expresses the internal density of the HPT at time t, T_{HPT} indicates the storage temperature of HPT.

3.1.5. A-LPT model

The A-TC-CCES system uses Fe-MOR(0.25) as the adsorbent and sets it in advance in the A-LPT. Since Fe-MOR(0.25) can realize the CO_2 adsorption and desorption process under dynamic conditions, the macroscopic performance of the A-TC-CCES system is stable and balanced in the compressor and turbine flow rate at a relatively small CO_2 mass flow rate. Then the volume of A-LPT required is:

$$V_{A-LPT} = \frac{M_{co_2}}{\rho_{CO_2}\beta_{Fe-MOR(0.25)}} \tag{9}$$

where V_{A-LPT} is the volume required for A-LPT. $\beta_{Fe-MOR(0.25)}$ is the adsorption ratio, taken as 219 m^3/m^3 [41]. ρ_{CO_2} is the density of CO_2.

3.1.6. Turbine model

Also as a power machine, the turbine is used for the expansion of the working mass to do work. The working process can be regarded as the inverse process of the compressor, and its model is:

$$\eta_T = \frac{h_{in} - h_{out}}{h_{in} - h_{out,is}} \tag{10}$$

This system contains 3 turbines with the following output power:

$$\dot{W}_{T,i} = \dot{m}_{co_2,er}(h_{in,i} - h_{out,i}) \tag{11}$$

where $\dot{W}_{T,i}$ is the output power of the turbine stage i. $\dot{m}_{co_2,er}$ denotes the CO_2 mass flow rate during the energy release process.

3.2. Exergy analysis model

Exergy represents the maximum available energy of a stream unit under specific environmental conditions. Exergy analysis is an essential method to evaluate the thermodynamic performance and is mainly used to estimate the level of irreversible losses and energy utilization of the system. In the proposed system, the exergy values of each stream unit are [15]:

$$\dot{E}_k = \dot{m}_k[(h_k - h_0) - T_0(s_k - s_0)] \tag{12}$$

where $\dot{E}$ stands for exergy power, the symbol s represents the specific entropy value, and the subscripts k and 0 represent the serial number of the flow unit and the environmental state, respectively.

For a given system component, the exergy destruction is calculated as:

$$\dot{E}_{D,j} = \dot{E}_{Q,j} + \sum(\dot{E}_{in,j} - \dot{E}_{out,j}) - \dot{W}_j \tag{13}$$

in which j denotes the component number, D represents destruction.

Based on the Eqs. (12) and (13), the exergy destruction model of each component in the system is displayed in Table 1.

Table 1
A-TC-CCES system component exergy destruction model.

Component	Exergy destruction model
C1	$\dot{W}_{C1} + \dot{E}_1 - \dot{E}_2$
IC1	$\dot{E}_2 - \dot{E}_3 + \dot{E}_{19} - \dot{E}_{22}$
C2	$\dot{W}_{C2} + \dot{E}_3 - \dot{E}_4$
IC2	$\dot{E}_4 - \dot{E}_5 + \dot{E}_{18} - \dot{E}_{21}$
C3	$\dot{W}_{C3} + \dot{E}_5 - \dot{E}_6$
IC3	$\dot{E}_6 - \dot{E}_7 + \dot{E}_{17} - \dot{E}_{20}$
TV	$\dot{E}_8 - \dot{E}_9$
RH1	$\dot{E}_{27} - \dot{E}_{30} + \dot{E}_9 - \dot{E}_{10}$
T1	$\dot{E}_{10} - \dot{E}_{11} - \dot{W}_{T1}$
RH2	$\dot{E}_{26} - \dot{E}_{29} + \dot{E}_{11} - \dot{E}_{12}$
T2	$\dot{E}_{12} - \dot{E}_{13} - \dot{W}_{T2}$
RH3	$\dot{E}_{25} - \dot{E}_{28} + \dot{E}_{13} - \dot{E}_{14}$
T3	$\dot{E}_{14} - \dot{E}_{15} - \dot{W}_{T3}$

3.3. Performance criteria

3.3.1. Round trip efficiency

Round trip efficiency is commonly used to measure energy storage performance. It is defined as the ratio of net output power in the energy release stage to net input power in the energy storage stage [50]:

$$\eta_{RTE} = \frac{\dot{W}_{net,er}t_{er}}{\dot{W}_{net,es}t_{es}} \times 100\% \tag{14}$$

where the subscripts *es* and *er* represent the energy storage stage and the energy release stage, respectively.

3.3.2. Exergy efficiency

The exergy efficiency reflects the level of energy utilization of the system. It is defined as [49]:

$$\eta_{EX} = 1 - \frac{\sum_{component}\dot{E}_D}{\dot{W}_{net,es}t_{es}} \tag{15}$$

3.3.3. Energy storage density

The energy storage density represents the net output per unit volume of work mass. Considering that the proposed system consists of 2 tanks, the energy storage density is defined as [34]:

$$EVR = \frac{\dot{W}_{net,er}t_{er}}{V_{A-LPT} + V_{HPT}} \tag{16}$$

3.4. Model validation

The system presented in this paper is a novel concept and has not been verified in engineering. To ensure the accuracy of the simulation, the device model is compared with that in the literature, and the results are shown in Table 2. The error is less than 1 % when compared with the equipment model in the literature, which proves the accuracy of the model in this paper. [22,47].

4. Results and discussion

4.1. Design working conditions

To verify the system performance, the system parameters were set based on published literature. The main design parameters are shown in Table 3.

Table 4 and Table 5 show the performance of the system and the state parameters under the design conditions shown in Table 3, respectively. The compressors consume 3537.4kWh of low valley electricity during the period when CO_2 was compressed from 0.1 MPa to 10 MPa. Compression heat is absorbed by the cold water and stored in the hot tank. In the energy release stage, the CO_2 is depressurized to 8 MPa by the throttle valve. before absorbing reheat, it enters the turbine and expands to do work, generating 2358.57 kWh of electricity. Round-trip efficiency value is 66.68 % at the design conditions. In the whole cycle,

Table 2
Model validation comparison results.

Component	State	P (MPa)			T (K)		
		Ref	Model	Error (%)	Ref	Model	Error (%)
Compressor [22]	1	1.480	1.480	0	297.15	297.15	0
	2	4.441	4.441	0	393.55	392.60	0.24
Turbine [22]	12	6.119	6.119	0	668.15	668.15	0
	13	2.000	2.000	0	558.35	561.40	0.55
Throttle valve [22]	15	1.980	1.980	0	302.65	302.65	0
	1	1.480	1.480	0	297.15	297.23	0.027
Heat exchanger [47]	2	14.141	14.141	0	566.27	566.27	0
	13	10	10	0	293.72	293.72	0
	3	14	14	0	328.374	328.373	−0.0003
	14	9.9	9.9	0	517.616	518.408	0.15

Table 3
Design conditions parameters of A-TC-CCES.

Parameter	Unit	Value
Ambient temperature	K	298 [28]
Ambient pressure	MPa	0.1 [28]
Cold water temperature	K	298.15 [22]
Water pump outlet pressure	MPa	2
Compressor inlet pressure	MPa	0.1
Energy storage pressure	MPa	10
HPT storage temperature	K	313.15
Isentropic efficiency of compressor	/	0.89 [51]
Isentropic efficiency of turbine	/	0.9 [21,28,51]
Effectiveness of heat exchanger	/	0.8 [47]
Mass flow rate of CO_2	kg/s	5
Duration of energy storage	h	2
Duration of energy release	h	2
Storage pressure of A-LPT	MPa	0.1
Adsorbent materials for A-LPT	/	Fe-MOR(0.25) [41]
Adsorbent performance	m^3/m^3	219 [41]

Table 4
System performance under design conditions.

Parameter	Unit	Value
V_{A-LPT}	m^3	92.07
V_{HPT}	m^3	102.65
$\dot{W}_C$	kWh	3537.40
$\dot{W}_T$	kWh	2358.57
$\dot{E}_D$	kWh	1139.48
η_{RTE}	/	66.68 %
η_{EX}	/	67.79 %
EVR	kWh/m^3	12.11

Table 5
Thermal parameters of the flow unit of the system under design conditions.

Stream	p (MPa)	T(K)	$\dot{m}$(kg/s)	Stream	p (MPa)	T(K)	$\dot{m}$(kg/s)
1	0.1	298.15	5	17	2.0	298.15	2.51
2	0.46	425.9	5	18	2.0	298.15	1.18
3	0.46	324.77	5	19	2.0	298.15	1.1
4	2.15	461.02	5	20	2.0	440.72	2.51
5	2.15	330.33	5	21	2.0	429.38	1.18
6	10.0	474.78	5	22	2.0	400.74	1.1
7	10.0	316.07	5	23	2.0	428.99	4.79
8	10.0	313.15	5	24	2.0	428.99	4.95
9	8.0	306.74	5	25	2.0	428.99	1.1
10	8.0	383.67	5	26	2.0	428.99	1.18
11	1.86	276.98	5	27	2.0	428.99	2.67
12	1.86	398.68	5	28	2.0	326.19	1.1
13	0.43	300.17	5	29	2.0	307.6	1.18
14	0.43	404.27	5	30	2.0	331.44	2.67
15	0.1	307.32	5	31	2.0	324.81	4.95
16	2.0	298.15	4.79				

the total exergy destruction of the components is 1139.48kWh and the system exergy efficiency is 67.79 %. Under the conditions of mass flow rate of 5 kg/s and storage and release time of 2 h, a total of 36 tons of CO_2 are involved in the cycle. The volume of HPT is 102.65 m^3, the volume of A-LPT is 92.07 m^3, and the energy storage density is 12.11 kWh/m^3. The above results suggest that the utilization of Fe-MOR(0.25) can dramatically reduce the volume of low-pressure storage tanks and significantly enhance the energy storage density of the system.

Fig. 3 and Fig. 4 illustrate the dynamic charging and discharging processes of HPT under the design conditions, respectively. As shown in Fig. 3(a), the storage temperature is kept at 313.15 K during HPT inflation, but the internal pressure increases from 8 MPa to 10 MPa with the inflow of CO_2. As shown in Fig. 3(b), the internal specific enthalpy of HPT decreases from 402.9 kJ/kg to 313.04 kJ/kg during the inflation process, while the specific thermodynamic energy decreases from 374.11 kJ/kg to 297.13 kJ/kg. Accordingly, as shown in Fig. 4, during the pressure drop from 10 MPa to 8 MPa inside the HPT, the storage temperature remains constant, and the internal specific enthalpy and specific thermodynamic energy return to the original state. After the above steps, the HPT completes a single cycle, and the dynamic calculation results verify its operational reliability.

Fig. 5 shows the results of exergy destruction analysis of system components under design conditions. The exergy destruction value of RH1 is 136.63 kW, accounting for 23.98 % of the total exergy destruction. The main reason is that the temperature of hot water is 428.99 K and the temperature of CO_2 is 306.74 K, thus the temperature difference between hot and cold fluids is large, resulting in a largely irreversible loss of RH1. In addition, from Fig. 5, it can be regarded that the compressor group has 7.17 %, 7.75 %, and 7.86 % of the exergy destruction, and the turbine group has 7.16 %, 8.13 %, and 8.29 % of the exergy destruction. Which demonstrates that the difference between the exergy destruction of power equipment is relatively small, and the heat exchanger is the component with greater change in exergy destruction.

4.2. Sensitivity analysis

The simulation results of the design conditions reveal that the system has the advantages of high round trip efficiency, high exergy efficiency and high energy storage density, which powerfully prove the feasibility of the proposed system. To further specify the effect of the parameters on the system performance, a sensitivity analysis study is conducted in this section. The key parameters can be identified by analyzing storage pressure, storage temperature, release pressure, heat exchanger effectiveness, compressor isentropic efficiency, and turbine isentropic efficiency. When investigating the effect of a specific parameter change on the system, the other parameters remain the same as the values listed in Table 3. The range of parameter variation is exhibited in Table 6.

4.2.1. Effect of storage pressure

Fig. 6 reveals the effect of storage pressure on the system. Fig. 6(a) shows the influence of storage pressure on the power of the equipment.

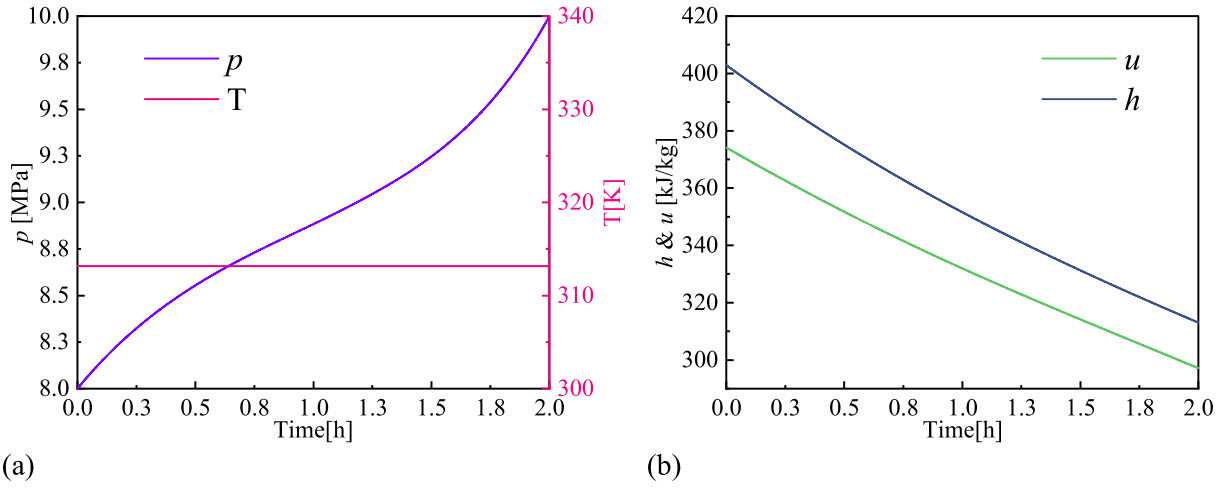

Fig. 3. Variation of HPT parameters during the energy storage stage: (a) pressure and temperature; (b) specific enthalpy and specific thermodynamic energy.

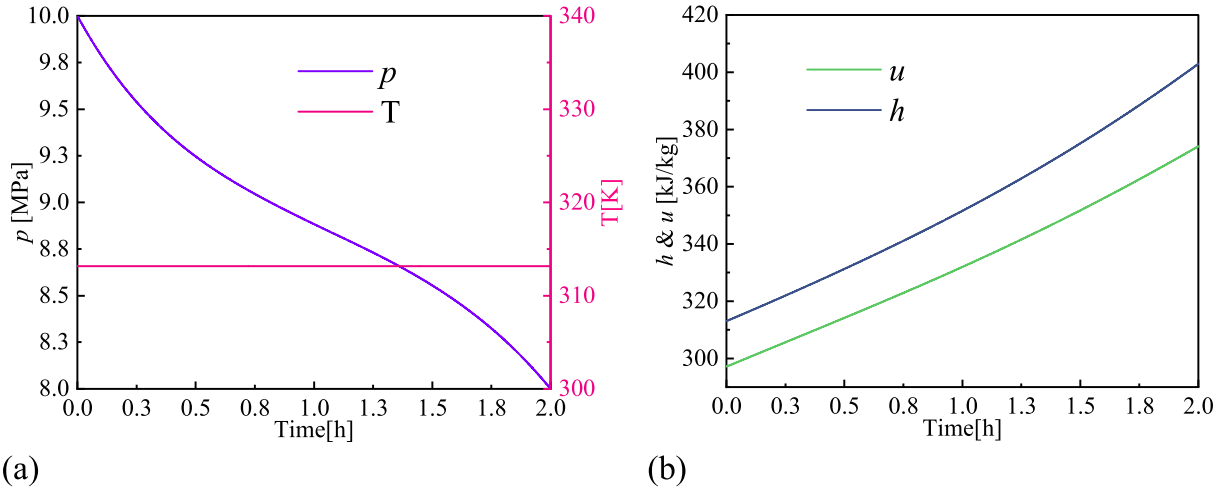

Fig. 4. Variation of HTP parameters during the energy release stage: (a) pressure and temperature; (b) specific enthalpy and specific thermodynamic energy.

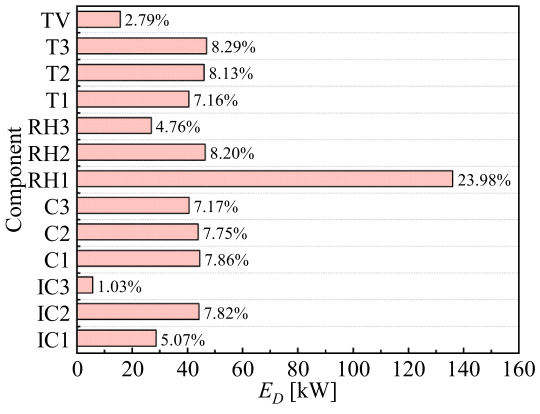

Fig. 5. Exergy destruction value of components at design conditions.

As the storage pressure increases from 10 MPa to 20 MPa, the power of the compressors, turbines, and total exergy destruction increase by 306.34 kW, 70.22 kW, and 233.81 kW, respectively. The main reason is that the compressor pressure ratio increases due to the rising storage pressure. And the compressor outlet pressure and temperature both increase, which directly leads to the increase in compressor power consumption. The compressor outlet temperature elevates the hot water temperature, which will enhance the turbine inlet temperature in the energy release stage and indirectly increase the turbine power output. Fig. 6(b) exhibits the effect of storage pressure on the volume of the tanks. The storage pressure increases by 12 MPa, while the release pressure remains unchanged, reduces the volume of the high-pressure tank by 38.58 m^3. Fig. 6(c) presents the effect of storage pressure on round-trip efficiency, exergy efficiency, and energy storage density. As the compressor power consumption increases more than the turbine output power and the total exergy destruction, the round-trip and exergy efficiency decrease by 6.47 % and 6.53 %, respectively. In addition, the energy storage density increases by 3.9 kWh/m^3 due to the combined effect of turbine power increase and tank volume reduction. Fig. 6(d) shows the effect of storage pressure on the exergy destruction of the components. With the improvement of storage pressure, the exergy

Table 6
Sensitivity analysis parameters range.

Parameter	Unit	Range	Step
Storage pressure	MPa	10–20	1
Storage temperature	K	310–320	1
Release pressure	MPa	5–9	1
Heat exchanger effectiveness	/	0.8–0.9	0.01
Compressor isentropic efficiency	/	0.7–0.9	0.02
Turbine isentropic efficiency	/	0.7–0.9	0.02

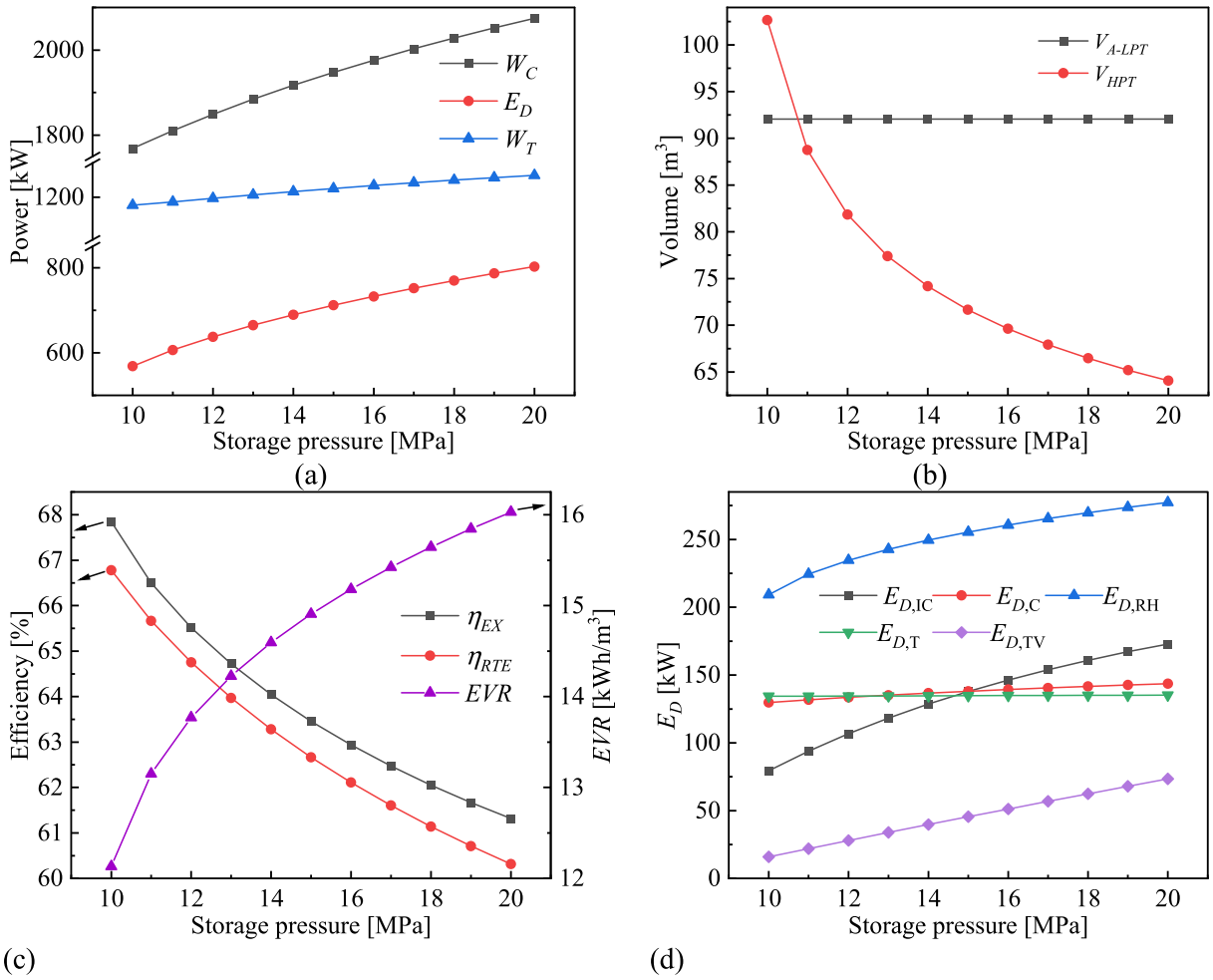

Fig. 6. Effect of storage pressure on system: (a) equipment power; (b) volume of tanks; (c) system performance; (d) exergy destruction of components.

destruction of intercoolers, reheaters, and the throttle valve increase by 93.52 kW, 68.07 kW, and 57.57 kW, respectively. The reason is that the increase in storage pressure raises the compressor pressure ratio and the compressor outlet temperature, which causes the increase in heat transfer temperature difference between intercoolers and reheaters and the exergy destruction increase. And the throttle valve import and export pressure difference increased from 2 MPa to 12 MPa, and the irreversible loss gradually increase.

4.2.2. *Effect of storage temperature*

Fig. 7 exhibits the effect of storage temperature on the system. Fig. 7 (a) illustrates the impact of storage temperature on the power of the devices. In the storage temperature range from 310 K to 320 K, the compressor power remains constant at 1768.7 kW, while the turbine power increases by 20.49 kW and the total exergy destruction decreases by 58.28 kW. Because the operating condition of the compression side components are not related to the storage temperature. However, the increase in storage temperature improves the throttle valve outlet temperature, reheater inlet temperature, and turbine inlet temperature, and thus increases the turbine power. At the same time, the temperature difference between the hot and cold streams of the reheaters reduce, and the general exergy destruction also reduces. Fig. 7(b) shows the effect of storage temperature on the volume of the storage tank. It can be seen from the figure that the volume of HPT decreases first and then increases. The main reason is that the storage temperature increases, which leads to the kinetic energy of CO_2 molecules increasing, and the intermolecular distance also increases. The macroscopic manifestation is the growth of the storage tank volume, which reaches 166.38 m^3 at 320 K. Fig. 7(c) represents the effect of storage temperature on round-trip efficiency, exergy efficiency, and energy storage density. Due to the constant compressor power, the increasing turbine power, and the decreasing total exergy destruction as storage temperature increases, round-trip efficiency and exergy efficiency increase by 1.16 % and 3.3 %, respectively. The energy storage density increases and then decreases with the synergistic effect of compressor power and tank volume. The maximum and minimum value are 12.31 kWh/m^3 and 9.26 kWh/m^3, respectively. Fig. 7(d) indicates the effect of storage temperature on the exergy destruction of components. The compressor and intercooler exergy destruction remain unchanged, but the reheater exergy destruction decreases by 67.34 kW, the turbine exergy destruction increases by 0.79 kW, and the throttle exergy destruction increases by 8.27 kW. The results suggest that the change in storage temperature mainly affects the energy release process.

4.2.3. *Effects of release pressure*

Fig. 8 displays the effect of the release pressure on the system. Fig. 8 (a) exhibits the impact of the release pressure on the power of the equipment, where the compressor power is constant for a release pressure in the range of 5–9 MPa. While the turbine power shows a trend of the first increase, then decrease and then increase, and the total exergy destruction shows a trend of first increase and then decreases. Moreover, the compressor and overall exergy destruction decreases and increases 6.36 kW and 58.5 kW at 7–7.5 MPa, respectively. The reason is that the trans-critical process of CO_2 occurs around 7.38 MPa, resulting in a sudden change of CO_2 physical parameters. Fig. 7(b) provides the effect of release pressure on the tank volume. As the release pressure increases,

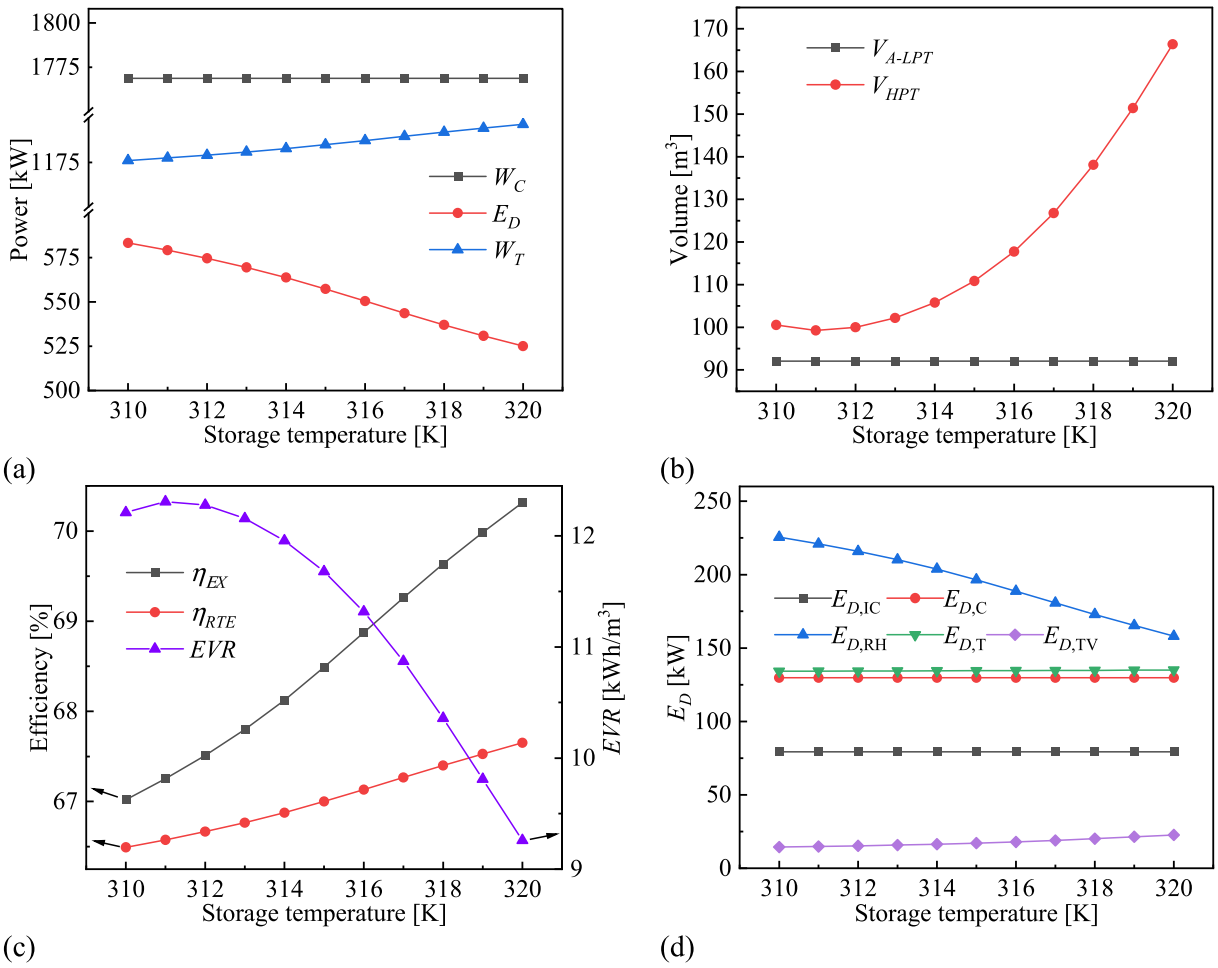

Fig. 7. Effect of storage temperature on system: (a) equipment power; (b) volume of tanks; (c) system performance; (d) exergy destruction of components.

the difference of storage and release pressure decreases continuously, resulting in an increase of 181.73 m^3 in the high-pressure tank volume, and the change rate increases gradually. Likewise, Fig. 8(c) represents the effect of release pressure on system performance, as turbine power and total exergy destruction change abruptly at 7–7.5 MPa, resulting in decrease in exergy efficiency and round-trip efficiency by 3.31 % and 0.36 %, respectively. Under the synergistic effect of turbine power and volume of HPT, the energy storage density decreases by a total of 6.91 kWh/m^3. Fig. 7(d) shows the effect of release pressure on the exergy destruction of the equipment. As shown, the total exergy destruction of the compressors and intercoolers remain unchanged, while the reheater exergy destruction shows a trend of increasing and then decreasing, and increases by 61.62 kW at 7–7.5 MPa. The total exergy destruction of the throttle valve decreases by 43.17 kW due to the decreasing differential pressure between inlet and outlet. The turbine exergy destruction increases by 16.62 kW during the whole process. The above analysis proves that the release pressure variation only affects the energy release stage.

4.2.4. *Effect of heat exchanger effectiveness*

Fig. 9 depicts the effect of heat exchanger effectiveness on the system. Fig. 9(a) shows the influence of heat exchanger effectiveness on equipment power. During the heat exchanger effectiveness upgrades from 0.8 to 0.9, the compressor power and total exergy destruction decrease by 66.97 kW and 66.47 kW, respectively, but the turbine power increases by 79.01 kW. The reason is that the compressor inlet temperature decreases due to the increase in heat exchanger effectiveness, and the compressor power consumption decreases. The inlet temperature of the turbine increases with the rising of heat exchanger effectiveness, which increases the turbine output power. At the same time, the heat exchanger effectiveness improves, the irreversible loss inside the heat exchanger decreases, and the total exergy destruction reduces. As shown in Fig. 8(b), the tank volume is not related to the heat exchanger's effectiveness. Fig. 8(c) presents the effect of heat exchanger efficiency on system performance, as shown in the figure, the exergy efficiency and round-trip efficiency vary almost linearly, and for every 0.01 increase in heat exchanger efficiency, the exergy efficiency and round-trip efficiency increase by 0.26 % and 0.73 %, respectively. Since the volume of the storage tanks remain unchanged, the turbine power increases linearly. The energy storage density also tends to increase gradually, with a total increase of 0.81 kWh/m^3. Fig. 8(d) shows the effect of heat exchanger effectiveness on the exergy destruction of the devices, the sum exergy destruction of the reheaters reduces by a total of 64.35 kW, with the exergy destruction of the rest of the devices remains almost the same, because the heat exchanger effectiveness increases, the end difference between the cold and hot streams decreases, and the irreversible losses of the reheaters also decrease. The above analysis proves that the change in heat exchanger effectiveness has significant influence on the energy storage process and energy release process, while there is no impact on the volume of the storage tank.

4.2.5. *Effect of compressor and turbine isentropic efficiency*

Fig. 10 indicates the synergistic effect of compressor and turbine isentropic efficiencies on the power of equipment. By increasing the compressor isentropic efficiency from 0.7 to 0.9, the compressor power decreases by 542.32 kW. Furthermore, the compressor power is not

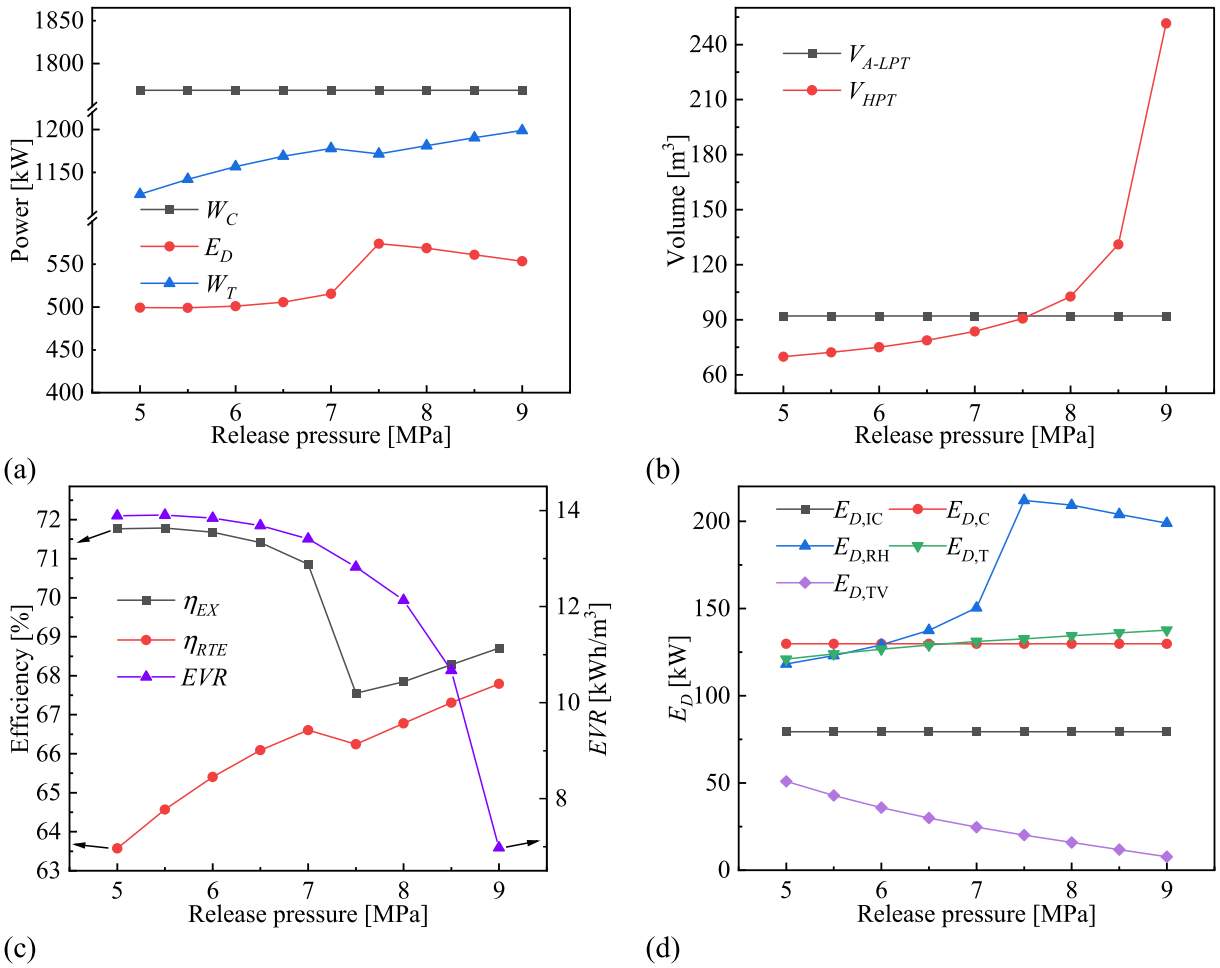

Fig. 8. Effect of release pressure on system: (a) equipment power; (b) volume of tanks; (c) system performance; (d) exergy destruction of components.

affected by the turbine's isentropic efficiency. Nevertheless, the increase in compressor isentropic efficiency hurts the turbine power. The cause is that the compressor isentropic efficiency increases, the compressor outlet temperature decreases, the hot water temperature decreases, and the turbine inlet temperature decreases, causing the turbine power to reduce. The maximum turbine power is 1263.38 kW when the compressor and turbine isentropic efficiencies are 0.7 and 0.9, respectively. The lowest turbine power is 922.09 kW when the compressor and turbine isentropic efficiencies are 0.9 and 0.7, respectively. By increasing the efficiency of the compressor and turbine, the total exergy destruction of the system reduces. When the entropy efficiency of both compressor and turbine is 0.7, the total exergy destruction is 1176.59 kW. When the entropy efficiency of both compressor and turbine is 0.9, the total exergy destruction is 552.99 kW, which decreases relatively by 53 %.

Fig. 11 illustrates the synergistic effect of compressor and turbine isentropic efficiency on the system performance. As shown in Fig. 11(a), the round-trip and exergy efficiency both rise with the increase of the two parameters. In the range from (0.7, 0.7) to (0.9, 0.9), the round-trip efficiency increases by 24.12 %, and the exergy efficiency increases by 19.74 %. Fig. 11(b) shows the combined effect of compressor and turbine isentropic efficiencies on energy storage density. The energy storage density decreases with increasing the compressor isentropic efficiency but increases with rising turbine isentropic efficiency. With compressor and turbine entropy efficiencies of 0.7 and 0.9, the energy storage density is 12.98 kWh/m^3. The lowest energy storage density is 9.47 kWh/m^3 when the compressor and turbine isentropic efficiencies are 0.9 and 0.7, respectively. The above analysis demonstrates that the compressor and turbine isentropic efficiencies have a synergistic effect on the system performance, and the system efficiency increases as both parameters increase. The system efficiency increases as both parameters improve. But the energy storage density decreases with the increase in compressor isentropic efficiency.

4.3. System comparison

In this section, a comprehensive comparison between the A-TC-CCES proposed in this paper and the TC-CCES presented by Hao et al. [20,49] is conducted. Fig. 12 illustrates the structure of TC-CCES. The round-trip efficiency and energy storage density of A-TC-CCES is 66.68 % and 12.11 kWh/m^3, respectively, under design conditions, while the indexes of TC-CCES are 66 % and 2.12 kWh/m^3, respectively. The energy storage density of A-TC-CCES is 5.71 times that of TC-CCES, with comparable round-trip efficiency. Furthermore, the pressure range of TC-CCES is 1–17 MPa, and the pressure range of the A-TC-CCES is 0.1–10 MPa, which requires less material strength for HPT and lower system operation and maintenance costs. More importantly, TC-CCES stores low-pressure CO_2 directly in large underground caves, which causes the system strictly depends on the geographical environment. In contrast, A-TC-CCES, based on an adsorption strategy, can achieve the storage density of CO_2 of 390.94 kg/m^3 at 0.1 MPa, and the system can be free from geographical constraints, with better prospects for industrial applications. From the above comparative analysis, A-TC-CCES is non-polluting, does not depend on specific geography, has a lower pressure range, and is more feasible.

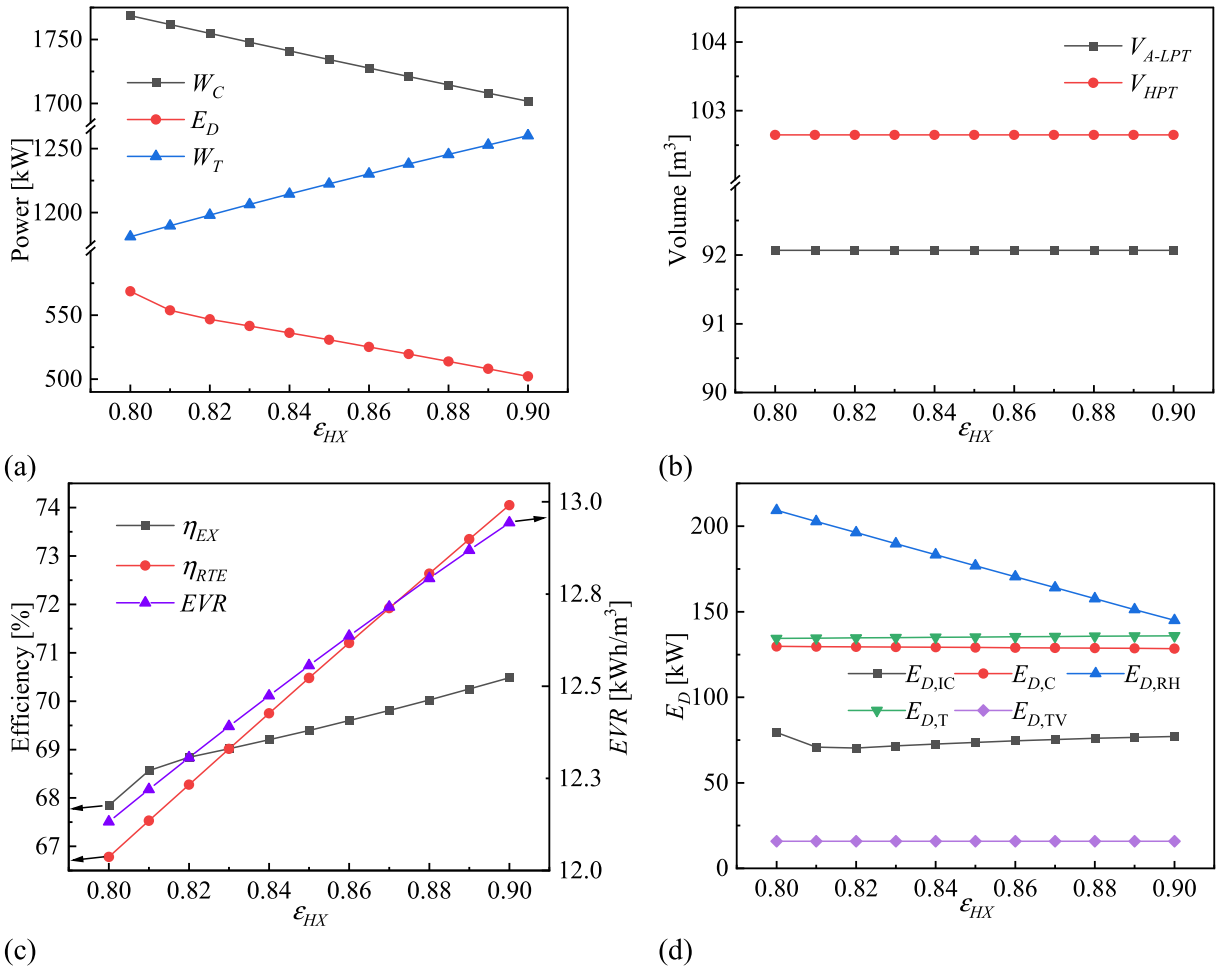

Fig. 9. Effect of heat exchanger effectiveness on system: (a) equipment power; (b) volume of tanks; (c) system performance; (d) exergy destruction of components.

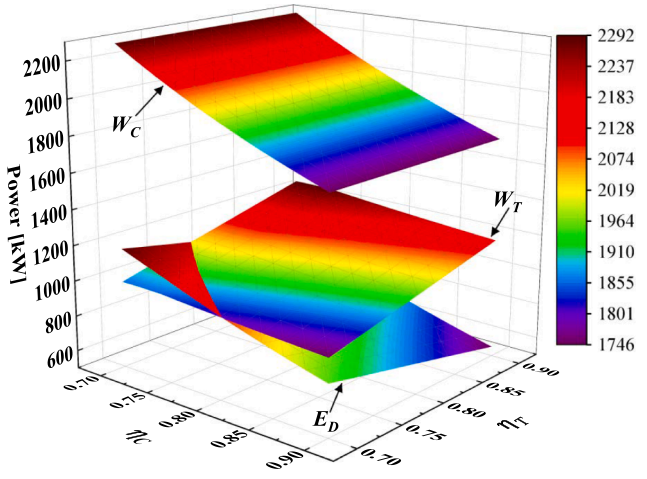

Fig. 10. Compressor and turbine isentropic efficiency on equipment power.

5. Conclusions

This paper proposes an adsorption type trans-critical compressed CO_2 energy storage system, which can significantly improve the system energy storage density with the low-pressure CO_2 adsorption strategy. A sensitivity analysis study is conducted to investigate the effect of crucial parameters on system performance indexes. The main conclusions can be drawn based on the current research as follows:

(1) The exergy efficiency, round-trip efficiency, and energy storage density of the proposed system are 67.79 %, 66.68 %, and 12.11 kWh/m^3 at the design conditions. The exergy destruction of the first-stage reheater is the largest, accounting for 23.98 %. Under the design conditions, the required volumes of A-LPT and HPT are 92.07 m^3 and 102.65 m^3, respectively.

(2) As the storage pressure increases, the system exergy and round-trip efficiency decrease, but the energy storage density increases. Besides, the rising storage pressure increases the exergy destruction of all components. As the storage temperature increases, the turbine power increases, while the volume of HPT first reduces and then increases, which ultimately leads to higher round-trip and exergy efficiency, while the storage density tends to increase and then decrease. The storage pressure and storage temperature have compound effects on the system.

(3) With the increase of the release pressure, the exergy destruction of the reheaters increases abruptly around the critical pressure (7.38 MPa), where the turbine power decreases suddenly, resulting in a sudden decrease in both round-trip and exergy efficiency. And with the increase of release pressure, the volume of HPT increases continuously, causing the energy storage density to drop sharply, and the gap between the highest and lowest energy storage density can reach 6.91 kWh/m^3.

(4) The heat exchanger's effectiveness has no impact on the volume of the storage tanks. However, an increase in heat exchanger effectiveness results in a linear increase in turbine output power and a linear decrease in compressor input power, ultimately causing a linear growth in round-trip efficiency and energy

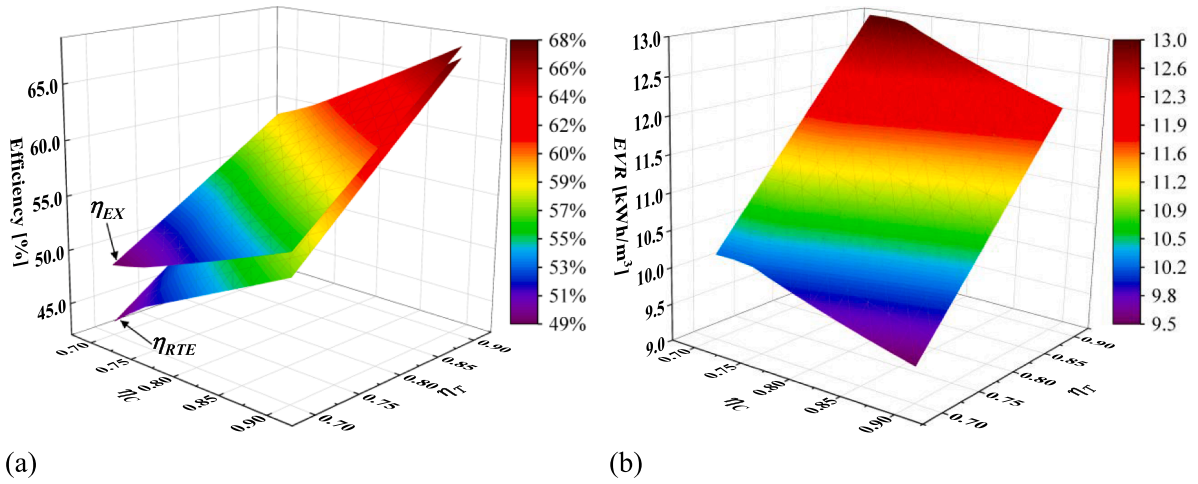

Fig. 11. Compressor and turbine equal entropy efficiency on system performance: (a) system efficiency; (b) energy storage density.

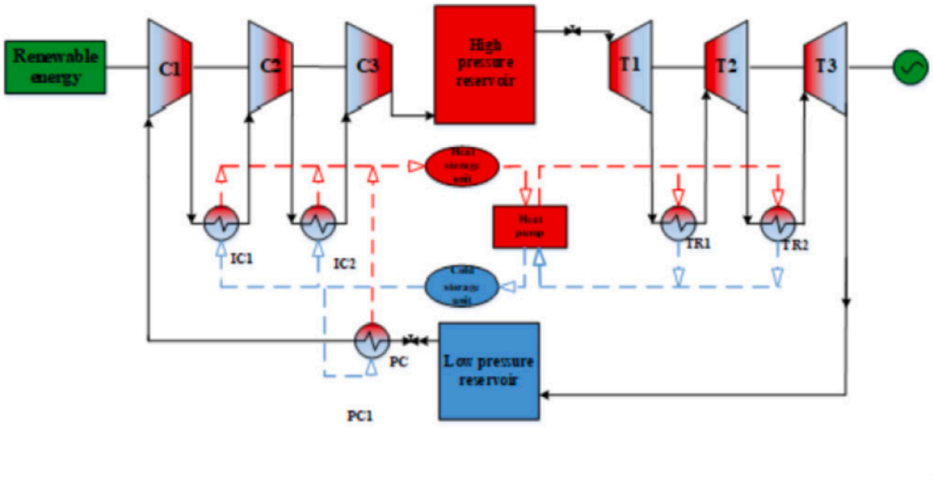

Fig. 12. Configuration schematic of TC-CCES [20,49].

storage density. Furthermore, an increase in heat exchanger effectiveness will result in a dramatic decrease in reheater exergy destruction.

(5) When increasing the isentropic efficiency of the compressor and turbine from 0.7 to 0.9, the round-trip efficiency and exergy efficiency increase by 24.12 % and 19.74 %, respectively. There is a peak value for energy storage density of 12.98 kWh/m^3 when the isentropic efficiencies of the compressor and turbine are 0.7 and 0.9, respectively. The increase in the isentropic efficiency of the compressor and turbine has positive effects on improving the system efficiency. However, the increase in the isentropic efficiency of compressors harms improving the energy storage density.

This paper presents an adsorption type compressed CO_2 energy storage system. To accurately simulate the system performance, energy analysis and exergy analysis are carried out based on the laws of thermodynamics. Energy analysis proves that the system has high energy storage density and is of great value for engineering applications. Exergy analysis identifies components with high available energy losses and provides fundamental data for subsequent system optimization. For practical applications, futural research should include adsorbent bed design, system optimization, and dynamic operation scheme design.

CRediT authorship contribution statement

Tianhang Zhang: Methodology, Formal analysis, Investigation, Data curation, Writing – original draft, Writing – review & editing. **Jianmin Gao:** Conceptualization, Validation, Supervision. **Yu Zhang:** Validation, Supervision. **Jin Zhang:** Methodology, Investigation. **Qiaoqun Sun:** Conceptualization, Validation. **Qian Du:** Project administration. **Zhipei Tang:** Writing – review & editing. **Yirui Peng:** Writing – review & editing.

Declaration of Competing Interest

The authors declare that they have no known competing financial interests or personal relationships that could have appeared to influence the work reported in this paper.

Data availability

No data was used for the research described in the article.

Acknowledgement

This work is supported by the 2022 Heilongjiang Province's "Emission and carbon neutrality" the open competition mechanism to select the best candidates project (Adsorption-type compression of carbon

dioxide energy storage key technology research and demonstration).

References

[1] Lund H, Salgi G. The role of compressed air energy storage (CAES) in future sustainable energy systems. Energy Convers Manage 2009;50:1172–9.
[2] Liu H, Yu D, Wang R, Aa A, Nojavan S, Jermsittiparsert K. Risk management of a renewable-based compressed air energy storage system using downside risk constraints approach. Renewable Energy 2020;161:470–81.
[3] Chen H, Peng Y-h, Wang Y-l, Zhang J. Thermodynamic analysis of an open type isothermal compressed air energy storage system based on hydraulic pump/turbine and spray cooling. Energy Convers Manage 2020;204:112293.
[4] Tsoukalas LH, Gao R. From smart grids to an energy internet: Assumptions, architectures and requirements. In: International Conference on Electric Utility Deregulation & Restructuring & Power Technologies; 2008. p. 94–8.
[5] Shams SA, Ahmadi R. Dynamic optimization of solarind hybrid system connected to electrical battery or hydrogen as an energy storage system. Int J Energy Res 2021;45:10630–54.
[6] B EMGRA, A RG, A SFS, A AWB, C JC, e JPSCad. Energy storage systems supporting increased penetration of renewables in islanded systems - ScienceDirect. Energy. 2014;75:265-80.
[7] Evans DJ, Carpenter G, Farr G. Mechanical systems for energy storage – scale and environmental issues. Pumped Hydroelectric and Compressed Air Energy Storage. Issues in environmental science and technology. 2018;46:42-114.
[8] Sivakumar N, Das D, Padhy NP. Economic analysis of Indian pumped storage schemes. Energy Convers Manage 2014;88:168–76.
[9] Fu H, He Q, Song J, Shi X, Liu W. Thermodynamic of a novel advanced adiabatic compressed air energy storage system with variable pressure ratio coupled organic rankine cycle. Energy 2021;120411.
[10] Zhao P, Gao L, Wang J, Dai Y. Energy efficiency analysis and off-design analysis of two different discharge modes for compressed air energy storage system using axial turbines. Renewable Energy 2016;85:1164–77.
[11] Dinter F, Geyer M, Tamme R. Thermal energy storage for commercial applications : a feasibility study on economic storage systems. Thermal energy storage for commercial applications : a feasibility study on economic storage systems. 1991.
[12] Luo X, Wang J, Dooner M, Clarke J, Krupke C. Overview of current development in compressed air energy storage technology. Energy Procedia 2014;62:603–11.
[13] Bullough C, Gatzen C, Jakiel C, Koller M, Zunft S. Advanced adiabatic compressed air energy storage for the Integration of wind energy. European Wind Energy Conf Ewec, November London UK; 2004.
[14] Pan L, Li B, Shi W, Wei X. Optimization of the self-condensing CO_2 transcritical power cycle using solar thermal energy. Appl Energy 2019;253.
[15] Sun W, Liu X, Yang X, Yang X, Liu Z. Design and thermodynamic performance analysis of a new liquid carbon dioxide energy storage system with low pressure stores. Energy Convers Manage 2021;239.
[16] Li Y, Yu H, Tang D, Li Y, Zhang G, Liu Y. A comparison of compressed carbon dioxide energy storage and compressed air energy storage in aquifers using numerical methods. Renewable Energy 2022;187:1130–53.
[17] Liu H, He Q, Borgia A, Pan L, Oldenburg CM. Thermodynamic analysis of a compressed carbon dioxide energy storage system using two saline aquifers at different depths as storage reservoirs. Energy Convers Manage 2016;127:149–59.
[18] Chaychizadeh F, Dehghandorost H, Aliabadi A, Taklifi A. Stochastic dynamic simulation of a novel hybrid thermal-compressed carbon dioxide energy storage system (T-CCES) integrated with a wind farm. Energy Convers Manage 2018;166:500–11.
[19] Cao Z, Deng J, Zhou S, He Y. Research on the feasibility of compressed carbon dioxide energy storage system with underground sequestration in antiquated mine goaf. Energy Convers Manage 2020;211.
[20] Hao Y, He Q, Du D. A trans-critical carbon dioxide energy storage system with heat pump to recover stored heat of compression. Renewable Energy 2020;152:1099–108.
[21] Akbari AD, Mahmoudi SMS. Thermoeconomic performance and optimization of a novel cogeneration system using carbon dioxide as working fluid. Energy Convers Manage 2017;145:265–77.
[22] Fu H, He Q, Song J, Hao Y. Thermodynamic of a novel solar heat storage compressed carbon dioxide energy storage system. Energy Convers Manage 2021;247.
[23] Xu M, Wang X, Wang Z, Zhao P, Dai Y. Preliminary design and performance assessment of compressed supercritical carbon dioxide energy storage system. Appl Therm Eng 2021;183:116153.
[24] Wang M, Zhao P, Wu Y, Dai Y. Performance analysis of a novel energy storage system based on liquid carbon dioxide. Appl Therm Eng 2015;91:812–23.
[25] Wang M, Zhao P, Yang Y, Dai Y. Performance analysis of energy storage system based on liquid carbon dioxide with different configurations. Energy 2015;93:1931–42.
[26] Zhang Y, Yang K, Hong H, Zhong X, Xu J. Thermodynamic analysis of a novel energy storage system with carbon dioxide as working fluid. Renewable Energy 2016;99:682–97.
[27] Zhang X-R, Wang G-B. Thermodynamic analysis of a novel energy storage system based on compressed CO_2fluid. Int J Energy Res 2017;41:1487–503.
[28] Liu Z, Yang X, Jia W, Li H, Yang X. Justification of CO_2 as the working fluid for a compressed gas energy storage system: A thermodynamic and economic study. J Storage Mater 2020;27.
[29] Liu Z, Liu Z, Xin X, Yang X. Proposal and assessment of a novel carbon dioxide energy storage system with electrical thermal storage and ejector condensing cycle: Energy and exergy analysis. Appl Energy 2020;269.
[30] Zhang Y, Liang T, Tian Z, Gao W, Yang K. A comprehensive parametric, energy and exergy analysis of a novel physical energy storage system based on carbon dioxide Brayton cycle, low-temperature thermal storage, and cold energy storage. Energy Convers Manage 2020;226.
[31] Zhang Y, Yao E, Zhang X, Yang K. Thermodynamic analysis of a novel compressed carbon dioxide energy storage system with low-temperature thermal storage. Int J Energy Res 2020;44:6531–54.
[32] Bao J, He X, Deng Y, Zhang N, Zhang X, An B, et al. Parametric analysis and multi-objective optimization of a new combined system of liquid carbon dioxide energy storage and liquid natural gas cold energy power generation. J Cleaner Prod 2022;363.
[33] Huang R, Zhou K, Liu Z. Reduction on the inefficiency of heat recovery storage in a compressed carbon dioxide energy storage system. Energy 2022;244.
[34] Liu Z, Liu X, Zhang W, Yang S, Li H, Yang X. Thermodynamic analysis on the feasibility of a liquid energy storage system using CO_2-based mixture as the working fluid. Energy 2022;238.
[35] Sun L, Tang B, Xie Y. Performance assessment of two compressed and liquid carbon dioxide energy storage systems: Thermodynamic, exergoeconomic analysis and multi-objective optimization. Energy 2022;256.
[36] Xu W, Zhao P, Gou F, Wu W, Liu A, Wang J. A combined heating and power system based on compressed carbon dioxide energy storage with carbon capture: Exploring the technical potential. Energy Convers Manage 2022;260.
[37] Chae YJ, Lee JI. Thermodynamic analysis of compressed and liquid carbon dioxide energy storage system integrated with steam cycle for flexible operation of thermal power plant. Energy Convers Manage 2022;256.
[38] Recent advances in solid sorbents for CO_2 capture and new development trends. Energy & Environ Sci 2014;7.
[39] Lanfang, Yujia, Yang, Xinyu, Wang, Xuan, et al. Porous Organic Polymers for Post-Combustion Carbon Capture.
[40] Oschatz M, Antonietti. A search for selectivity to enable CO_2 capture with porous adsorbents. Energy & environmental science: EES. 2018;11:57-70.
[41] Zhou Y, Zhang J, Wang L, Cui X, Wang J. Self-assembled iron-containing mordenite monolith for carbon dioxide sieving. Science (New York, NY).373:315-20.
[42] Liang L, Liu C, Jiang F, Chen Q, Zhang L, Xue H, et al. Carbon dioxide capture and conversion by an acid-base resistant metal-organic framework. Nat Commun 2017;8:1233.
[43] Liao PQ, Chen H, Zhou DD, Liu SY, He CT, Rui Z, et al. Monodentate hydroxide as a super strong yet reversible active site for CO_2 capture from high-humidity flue gas. Energy Environ Sci 2015;8:1011–6.
[44] Liu Z, Yang X, Liu X, Wang W, Yang X. Evaluation of a trigeneration system based on adiabatic compressed air energy storage and absorption heat pump: Thermodynamic analysis. Appl Energy 2021;300.
[45] Zhao P, Xu W, Gou F, Fan G, Wang J. Performance analysis of a self-condensation compressed carbon dioxide energy storage system with vortex tube. J Storage Mater 2021;41.
[46] Zhang Y, Yao E, Tian Z, Gao W, Yang K. Exergy destruction analysis of a low-temperature Compressed Carbon dioxide Energy Storage system based on conventional and advanced exergy methods. Appl Therm Eng 2021;185.
[47] Liu Z, Cao F, Guo J, Liu J, Zhai H, Duan Z. Performance analysis of a novel combined cooling, heating and power system based on carbon dioxide energy storage. Energy Convers Manage 2019;188:151–61.
[48] Liu Z, Liu X, Yang X, Yang X. Assessment of a new combined thermal and compressed energy storage coupled with an absorption power cycle: Thermodynamic study. Energy Convers Manage 2020;226.
[49] Hao Y, He Q, Liu W, Pan L, Oldenburg CM. Thermodynamic analysis of a novel fossil-fuel–free energy storage system with a transritical carbon dioxide cycle and heat pump. Int J Energy Res 2020.
[50] Han Z, Guo S. Investigation of discharge characteristics of a tri-generative system based on advanced adiabatic compressed air energy storage. Energy Convers Manage 2018;176:110–22.
[51] She X, Peng X, Nie B, Leng G, Zhang X, Weng L, et al. Enhancement of round trip efficiency of liquid air energy storage through effective utilization of heat of compression. Appl Energy 2017;206:1632–42.